

Deep VLT spectroscopy of the blue compact dwarf galaxies Tol 1214–277 and Tol 65^{*}

Y. I. Izotov¹, P. Papaderos², N. G. Guseva¹, K. J. Fricke², and T. X. Thuan³

¹ Main Astronomical Observatory, Ukrainian National Academy of Sciences, 27 Zabolotnoho str., Kyiv 03680, Ukraine

² Universitäts-Sternwarte, Geismarlandstraße 11, D-37083 Göttingen, Germany

³ Astronomy Department, University of Virginia, Charlottesville, VA 22903, USA

Received ; Accepted

Abstract. We present VLT spectroscopic observations with different spectral resolutions and different slit orientations of the two metal-deficient blue compact dwarf (BCD) galaxies Tol 1214–277 and Tol 65. The oxygen abundances in the brightest H II regions of Tol 1214–277 and Tol 65 are found to be $12 + \log O/H = 7.55 \pm 0.01$ and 7.54 ± 0.01 , or $Z_{\odot}/24^{**}$. The nitrogen-to-oxygen abundance ratios in the two galaxies are $\log N/O = -1.64 \pm 0.03$ and -1.60 ± 0.02 and lie in the narrow range found for other most metal-deficient BCDs. The helium mass fraction derived in several H II regions in both galaxies is consistent with a high primordial helium mass fraction, $Y_p \sim 0.244$. We confirm the detection of the high-ionization forbidden emission line [Fe v] $\lambda 4227$ in the spectrum of Tol 1214–277. Additionally, weak [Ne iv] $\lambda 4725$, [Fe vi] $\lambda 5146$, $\lambda 5177$, and [Fe vii] $\lambda 5721$, $\lambda 6087$ emission lines are detected in the high-resolution spectrum of Tol 1214–277. The detection of these lines implies the presence of hard radiation with photon energy in the range $\sim 4 - 8$ Ryd. Emission lines are detected in the spectra of eight galaxies in the fields of Tol 1214–277 and Tol 65. Seven of these galaxies are background objects, while one galaxy has a redshift close to that of Tol 1214–277. Situated at a projected distance of ~ 14.5 kpc from Tol 1214–277, this galaxy is probably a companion of the BCD.***

Key words. galaxies: starburst – galaxies: abundances – galaxies: individual (Tol 1214–277, Tol 65)

1. Introduction

Detailed spectroscopic studies of extremely metal-poor local blue compact dwarf (BCD) galaxies based on observations with large telescopes are useful to derive accurately their element abundances and shed light on the properties and origin of these galaxies. BCDs may be considered local counterparts to high-redshift nearly primordial star-forming galaxies because of their low metallicity and active star formation. Spectroscopic studies of other galaxies in the field of BCDs are aimed at searching for companion galaxies. Such a companion galaxy has been found, e.g. for the second most metal-deficient BCD known, SBS 0335–052, at a projected distance of ~ 22 kpc (Pustilnik et

al. 1997, 2001; Lipovetsky et al. 1999). The gravitational interaction between the galaxies in such pairs has been suggested as a triggering mechanism of star formation in BCDs (Pustilnik et al. 2001; Noeske et al. 2001).

We focus here on two BCDs, Tol 1214–277 \equiv Tol 21 and Tol 65 \equiv Tol 1223–359 \equiv ESO 380 – G027. Using deep VLT imaging of these BCDs, Fricke et al. (2001) and Papaderos et al. (1999) have studied their morphological properties. In Tol 1214–277, a very bright and compact star-forming region (region 1 in the inset of Fig. 1, left panel) at the north-eastern edge of the galaxy is embedded in a relatively blue extended low-surface-brightness (LSB) component with some other fainter star-forming regions (Fricke et al. 2001). As for Tol 65, Papaderos et al. (1999) have found several regions of star formation in the northern part (see inset in Fig. 1, right panel), also embedded in a relatively blue LSB component. The distances to Tol 1214–277 and Tol 65 are respectively 103.9 Mpc and 36.0 Mpc, using the observed radial velocities of 7795 km s^{-1} and 2698 km s^{-1} and assuming a Hubble constant $H_0 = 75 \text{ km s}^{-1} \text{ Mpc}^{-1}$ (Thuan & Izotov 1997). The presence of massive stars in these BCDs is indicated by strong nebular lines (Izotov et al. 2001a) and, in the

Send offprint requests to: izotov@mao.kiev.ua

^{*} Based on observations obtained at the European Southern Observatory, Paranal, Chile (ESO Programs 63.P-0003 and 65.N-0642)

^{**} $12 + \log(O/H)_{\odot} = 8.92$ (Anders & Grevesse 1989).

^{***} Tables 2, 3, 4 and 8 are also available in electronic form at the CDS via anonymous ftp to cdsarc.u-strasbg.fr (130.79.128.5) or via <http://cdsweb.u-strasbg.fr/cgi-bin/qcat?J/A+A/>

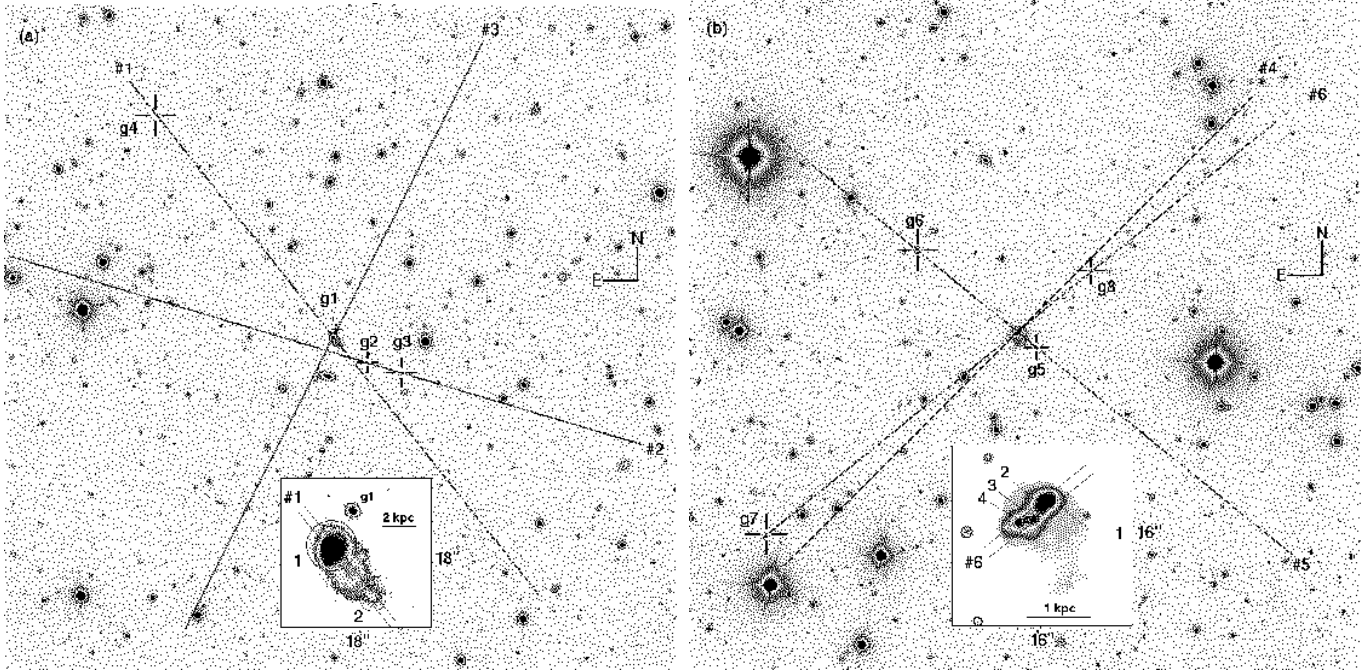


Fig. 1. Tol 1214–277 (left panel) and Tol 65 (right panel) centered on the VLT FORS1 6'8×6'8 field of view. The positions of the slits used for spectroscopic observations are shown by straight lines and are labeled #1 to #3 and #4 to #6, respectively. The insets display enlarged versions of the BCDs with the slits #1 and #6 overlaid on Tol 1214–277 and Tol 65, respectively. The H II regions 1 and 2 in Tol 1214–277 (left panel) and 1 to 4 in Tol 65 (right panel) are indicated.

Table 1. Journal of observations.

Field	Date	Slit #	Spectral elements	Spectral range	Slit	P.A.	Exposure	Airmass	Seeing
Tol 1214–277	18.05.1999	1	G300V + GG 375	3600–7400Å	1''	39°	2×660 s	1.7	0''69
	25.06.2000	1	G300V + GG 375	3600–7400Å	1''	39°	2×900 s	1.5	1''12
	28.06.2000	2	G300V + GG 375	3600–7400Å	1''	73°	2×900 s	1.5	1''04
	25.06.2000	3	G600B	3600–5400Å	1''	154°	3×900 s	1.1	1''33
	25.06.2000	3	G600R + GG 435	5300–7400Å	1''	154°	2×900 s	1.2	1''61
Tol 65	15.05.1999	4	G300V + GG 375	3600–7400Å	1''	135°	2×420 s	1.4	0''34
	30.06.2000	5	G300V + GG 375	3600–7400Å	1''	51°	2×900 s	1.6	0''80
	30.06.2000	6	G600B	3600–5400Å	1''	129°	3×900 s	1.2	0''96
	30.06.2000	6	G600R + GG 435	5300–7400Å	1''	129°	2×900 s	1.3	1''03

case of Tol 1214–277, by a UV stellar N v λ 1240 line with a P Cygni profile (Thuan & Izotov 1997).

The very low metallicity of Tol 1214–277 and Tol 65 has been established by earlier spectroscopic work (Kunth & Sargent 1983; Campbell, Terlevich & Melnick 1986; Pagel et al. 1992; Masegosa, Moles & Campos-Aguilar 1994). Recently, Fricke et al. (2001) and Izotov et al. (2001a) using VLT and Keck spectroscopic observations have derived the oxygen abundance $12 + \log O/H = 7.52$ and 7.54 in Tol 1214–277, and Izotov et al. (2001a) have found $12 + \log O/H = 7.54$ in Tol 65. Hence these two galaxies are the most metal-deficient BCDs known in the Southern hemisphere, after SBS 0335–052 with $12 + \log O/H = 7.30$ (Izotov et al. 1997b). We present here new VLT spectroscopic observations of these two BCDs to pursue two problems. The first one concerns the N/O abundance ratio. Pagel et al. (1992) have measured the

nitrogen-to-oxygen abundance ratio in Tol 65 to be $\log N/O = -1.81 \pm 0.15$, significantly lower than the mean value $\log N/O \approx -1.60 \pm 0.02$ obtained by Thuan et al. (1995) and Izotov & Thuan (1999) for low-metallicity BCDs with $12 + \log O/H \lesssim 7.6$. On the other hand, the N/O abundance ratio in Tol 1214–277 is similar to that of other BCDs. Recently, Izotov et al. (2001a) using low-resolution Keck spectra of Tol 1214–277 and Tol 65 have found $\log N/O = -1.64$ for both galaxies, more in line with other low-metallicity BCDs. To understand the origin of nitrogen in a low-metallicity environment (e.g., Meynet & Maeder 2002), it is important to check these results with new high-quality spectroscopic data with better spectral resolution.

The second problem concerns the nature of the hard radiation field in low-metallicity BCDs. Tol 1214–277 shows the strongest He II λ 4686 emission among all known

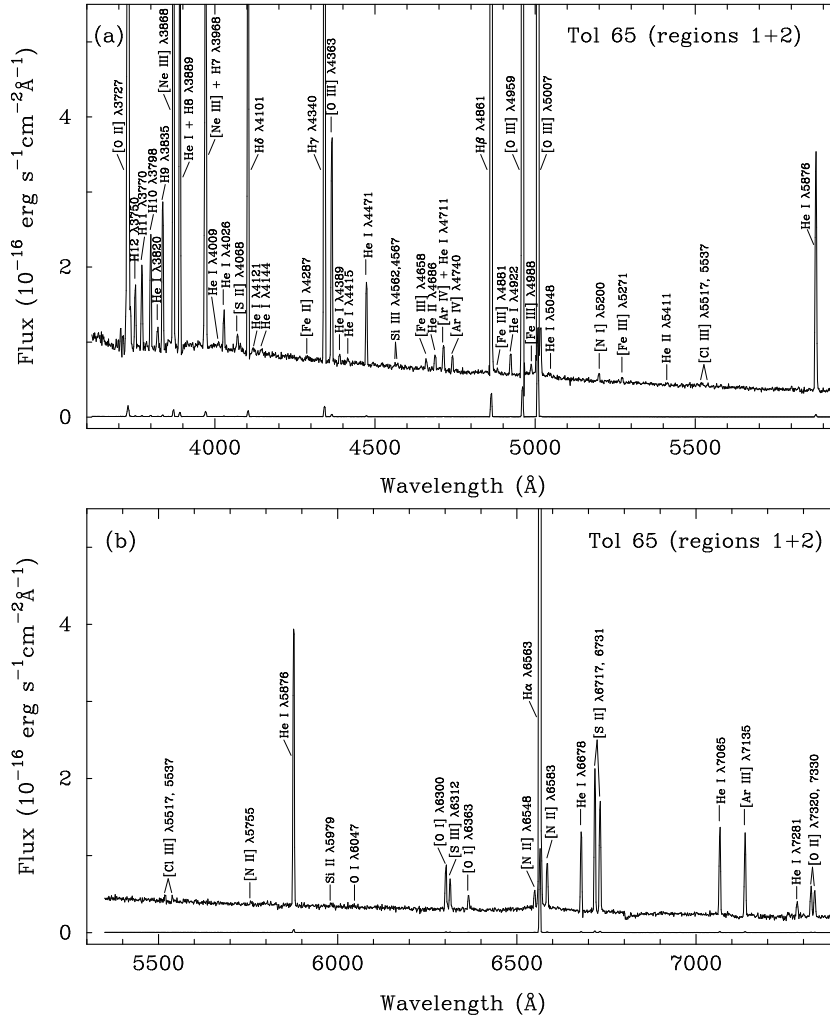


Fig. 3. Blue (a) and red (b) parts of the redshift-corrected high-resolution spectrum of regions 1 + 2 in Tol 65 obtained in 2000 with slit position #6. The emission lines are labeled. The lower spectra in (a) and (b) are the observed spectra downscaled by a factor of 100.

spectra in the red parts were obtained with a GG 435 second-order blocking filter. The spectral coverage was 3600 – 5400 Å in the blue and 5300 – 7400 Å in the red. A $1'' \times 400''$ slit was used for all observations. The airmass during the observations varied from 1.1 to 1.7. The positions of the slits were chosen to go through all brightest H II regions in both BCDs and some suspected emission-line galaxies in the fields of Tol 1214–277 and Tol 65 (Fig. 1, Table 1). With the total exposure times shown in Table 1, the spectra have a signal-to-noise ratio $S/N \gtrsim 50$ in the continuum of the brightest parts of the BCDs. They were broken up into two subexposures, to allow for cosmic-ray removal. A spectrum of a He-Ne-Ar comparison lamp was obtained for wavelength calibration.

Data reduction was carried out using the IRAF¹ software package. This included bias subtraction, cosmic-ray removal, flat-field correction, wavelength calibration and night-sky emission subtraction. Spectrophotometric stan-

dard stars were observed during the same nights with $2''$ wide slits. However, because of hardware problems of the spectrograph those spectra were shifted by ~ 300 pixels along the dispersion axis compared to object spectra, and were therefore unusable. The flux calibration was done using calibrated spectra of Tol 1214–277 and Tol 65 obtained previously by Izotov et al. (2001a) with the Keck telescope. For this, we removed the emission lines and obtained the continuum distributions for both the flux-calibrated Keck and uncalibrated VLT spectra. The transformation curve to flux-calibrate the VLT spectra is then obtained by dividing one continuum by the other.

3. Chemical abundances

We derive the element abundances in the brightest H II regions of Tol 1214–277 and Tol 65 using all available data obtained during the two periods of observations. The seeing during the observations varied over a wide range, from $0''.34$ to $1''.61$ (FWHM). We were able to extract one-dimensional spectra of all four regions from the low-

¹ IRAF: the Image Reduction and Analysis Facility is distributed by the National Optical Astronomy Observatory.

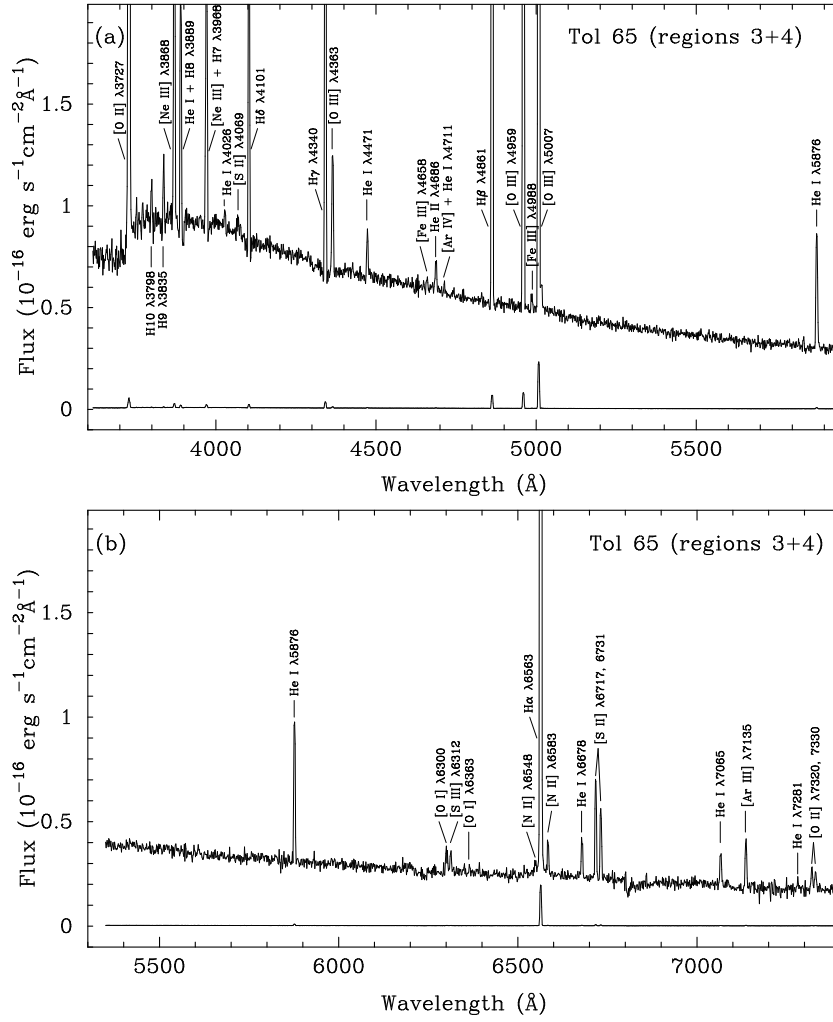


Fig. 4. Blue (a) and red (b) parts of the redshift-corrected high-resolution spectrum of regions 3 + 4 in Tol 65 obtained in 2000 with slit position #6. The emission lines are labeled. The lower spectra in (a) and (b) are the observed spectra downscaled by a factor of 100.

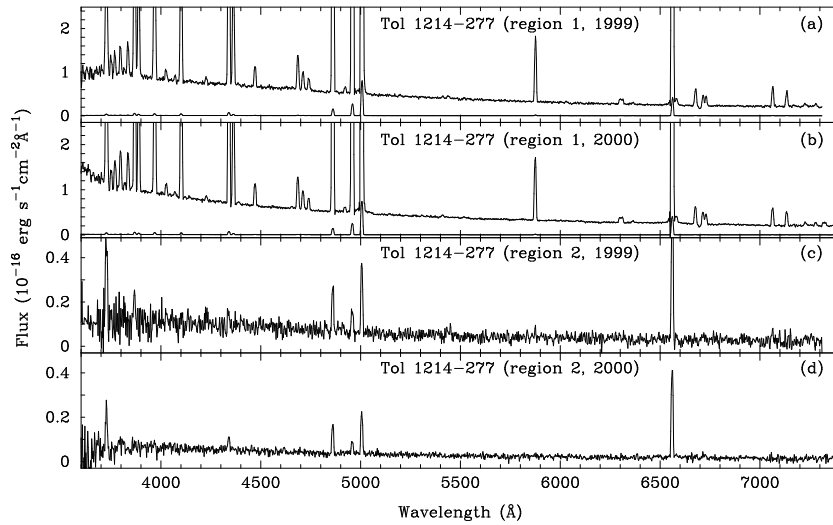


Fig. 5. Redshift-corrected low-resolution spectra of regions 1 and 2 in Tol 1214–277 obtained in 1999 and 2000 with slit position #1. The lower spectra in (a) and (b) are the observed spectra downscaled by a factor of 100.

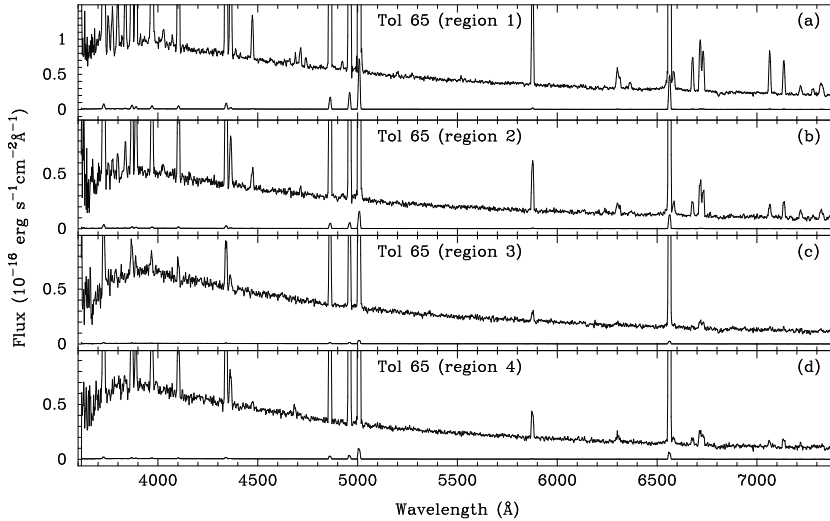


Fig. 6. Redshift-corrected low-resolution spectra of regions 1 – 4 in Tol 65 obtained in 1999 with slit position #4. The lower spectra are the observed spectra downsampled by a factor of 100.

resolution long-slit spectrum of Tol 65, obtained on 15 May 1999 (slit #4) with exceptionally good seeing ($0''.34$ FWHM). However, the seeing during the high-resolution spectroscopic observations of Tol 65 on 30 June, 2000 (slit #6) was not as good ($1''.03$ FWHM), so that we were able to extract only one-dimensional spectra for the combined regions (1+2) and (3+4). The one-dimensional spectra from the low-resolution long-slit spectrum of Tol 65 were extracted within an aperture of $1'' \times 1''$. In all other cases, the spectra were extracted within an aperture of $2'' \times 1''$.

The emission line fluxes were measured with the IRAF SPLOT routine using Gaussian profile fitting. The errors of the line fluxes are defined by the total photon counts in each line and are derived from the non-flux-calibrated spectra. They have been propagated in the calculations of the elemental abundance errors. Fluxes have been corrected for underlying stellar absorption (for hydrogen lines) and interstellar extinction using the observed Balmer decrement, following the procedure described by Izotov et al. (1994, 1997a). This is done by minimizing the deviations of the hydrogen emission line fluxes corrected for extinction and underlying absorption, from their theoretical values. All non-blended hydrogen emission lines were used. The Whitford (1958) reddening law was adopted.

3.1. Emission-line fluxes

3.1.1. High-resolution spectra

The spectrum of the brightest region 1 of Tol 1214–277 was obtained with slit #3 (Fig. 1), oriented roughly perpendicular to the major axis of the galaxy. It is shown in Fig. 2. The spectrum is dominated by very strong emission lines, reflecting the ongoing star formation activity. Because of the high signal-to-noise ratio and the high spectral resolution, several weak permitted and forbidden nebular emission lines are present in the spectrum. The emission lines

[O I] $\lambda 6300$ and [S III] $\lambda 6312$, H α $\lambda 6563$ and [N II] $\lambda 6583$ are well separated, allowing for a reliable determination of sulfur and nitrogen abundances. Remarkable spectral features are the nebular high-ionization He II $\lambda 4686$, $\lambda 5411$ and [Fe V] $\lambda 4227$ emission lines discussed by Fricke et al. (2001) and suggesting the presence of a very hard radiation with photon energies $\gtrsim 4$ Ryd in the BCD. In addition to these findings, we detect the [Ne IV] $\lambda 4725$ emission line and weak [Fe VI] $\lambda 5146$, $\lambda 5177$, [Fe VII] $\lambda 5721$, $\lambda 6087$ emission lines. This makes Tol 1214–277 the second known BCD, after SBS 0335–052 (Izotov et al. 2001b), with detected [Fe VI] – [Fe VII] emission lines.

The corrected fluxes $I(\lambda)/I(\text{H}\beta)$ and equivalent widths EW of emission lines together with the extinction coefficient $C(\text{H}\beta)$, the absolute flux $F(\text{H}\beta)$ of the H β emission line and the equivalent width $EW(\text{abs})$ of hydrogen absorption lines for region 1 of Tol 1214–277 are listed in Table 2.

The high resolution spectra of regions 1+2 and 3+4 in Tol 65 were obtained with slit #6 (Fig. 1) oriented along the chain of star-forming regions in the northern part of the galaxy and are shown, respectively, in Fig. 3 and 4. As for the spectrum of region 1 in Tol 1214–277, they are characterised by strong emission lines. However, the emission lines of the high ionization ions, except for the He II $\lambda 4686$ emission line, are not present in the spectra of these regions implying milder ionizing radiation as compared to Tol 1214–277. The corrected fluxes $I(\lambda)/I(\text{H}\beta)$ and the equivalent widths EW of emission lines together with the extinction coefficient $C(\text{H}\beta)$, the absolute flux $F(\text{H}\beta)$ of the H β emission line and the equivalent width $EW(\text{abs})$ of hydrogen absorption lines for regions 1+2 and 3+4 of Tol 65 are listed in Table 2. Note that the flux of the He II $\lambda 4686$ emission line relative to H β is stronger in the more evolved starbursts of regions 3+4, with lower equivalent width of H β , as compared to the younger bursts in regions 1+2.

We derive a redshift $z = 0.02603 \pm 0.00008$ for region 1 in Tol 1214–277 using the 44 brightest emission lines. As for Tol 65, redshifts $z = 0.00974 \pm 0.00010$ for regions 1+2, using the 40 brightest lines, and $z = 0.00966 \pm 0.00010$ of regions 3+4, using the 29 brightest lines, are obtained.

3.1.2. Low-resolution spectra

We show in Fig. 5 the low-resolution spectra of regions 1 and 2 in Tol 1214–277 obtained during the two 1999 and 2000 runs, with slit #1 (Fig. 1) oriented along the major axis of the galaxy. The corrected fluxes and equivalent widths of the emission lines are shown in Table 3. As in the case of the high-resolution spectra, the high-ionization He II $\lambda 4686$, $\lambda 5411$ and [Fe V] $\lambda 4227$ emission lines were also detected in region 1. The low spectral resolution precludes flux measurement of the [S III] $\lambda 6312$ emission line, blended with the [O I] $\lambda 6300$ emission line. Likewise, the [N II] $\lambda 6583$ emission line is blended with H α . The [N II] $\lambda 6583$ fluxes in the spectra of region 1 were therefore measured by setting the continuum at the top of the wing of the H α emission line. Region 2 is characterised by a blue spectrum, however only a few strongest emission lines with low equivalent widths are detected. The temperature-sensitive [O III] $\lambda 4363$ emission line is not seen, precluding a reliable abundance determination.

We show the four spectra of regions 1 to 4 in Tol 65 in Fig. 6. The corrected fluxes and equivalent widths of emission lines are shown in Table 4. Note that the observed H α /H β flux ratios in regions 3 and 4 are lower than the theoretical recombination value. This likely reflects uncertainties in the flux calibration of the Tol 65 spectrum. Therefore, for regions 3 and 4 we set the extinction coefficient $C(\text{H}\beta) = 0$. The high spatial resolution allows to identify more accurately the regions with He II $\lambda 4686$ emission. It is seen from Table 4 that the He II $\lambda 4686$ /H β flux ratio is small in region 1 and much larger in region 4. No He II emission is detected in regions 2 and 3. Hence, the ionization radiation is the hardest in region 4.

3.2. Heavy element abundances

To derive element abundances, we adopted a two-zone photoionized H II region model (Stasińska 1990) including a high-ionization zone with temperature $T_e(\text{O III})$, and a low-ionization zone with temperature $T_e(\text{O II})$. The electron temperature $T_e(\text{O III})$ is derived from the [O III] $\lambda 4363/(\lambda 4959 + \lambda 5007)$ ratio using a five-level atom model. That temperature is used for the derivation of the He⁺, He²⁺, O²⁺, Ne²⁺ and Ar³⁺ ionic abundances. $T_e(\text{O II})$ is obtained from $T_e(\text{O III})$ using the relation given in Izotov et al. (1994), based on a fit to the photoionization models of Stasińska (1990). The temperature $T_e(\text{O II})$ is used to derive the O⁺, N⁺, S⁺ and Fe²⁺ ion abundances. For S²⁺, Cl²⁺ and Ar²⁺ we have adopted an electron temperature intermediate between $T_e(\text{O III})$ and $T_e(\text{O II})$ following the prescriptions of Garnett (1992).

The oxygen abundance is derived as

$$\frac{\text{O}}{\text{H}} = \frac{\text{O}^+}{\text{H}^+} + \frac{\text{O}^{+2}}{\text{H}^+} + \frac{\text{O}^{+3}}{\text{H}^+}, \quad (1)$$

where

$$\frac{\text{O}^{+3}}{\text{H}^+} = \frac{\text{He}^{+2}}{\text{He}^+} \times \left(\frac{\text{O}^+}{\text{H}^+} + \frac{\text{O}^{+2}}{\text{H}^+} \right). \quad (2)$$

Total abundances of other heavy elements were computed after correction for unseen stages of ionization, as described in Izotov et al. (1994), Thuan et al. (1995) and Guseva et al. (2003).

3.2.1. High-resolution spectra

The heavy element abundances obtained from the high-resolution spectra of region 1 in Tol 1214–277 (slit #3) and of regions 1+2 and 3+4 in Tol 65 (slit #6) are shown in Table 5. We also show in this Table the electron temperatures $T_e(\text{O III})$, $T_e(\text{O II})$, and $T_e(\text{S III})$, the electron number density $N_e(\text{S II})$ and $N_e(\text{He II})$, and the ionization correction factors $\times \text{ICF}$ used for the abundance determination.

The oxygen abundances of Tol 1214–277 and Tol 65 are very similar. They are in general agreement with those obtained in previous studies.

The high spectral resolution allows us to determine the nitrogen abundance with great accuracy because the [N II] $\lambda 6583$ emission line is not blended with H α . The nitrogen-to-oxygen abundance ratios $\log \text{N/O} = -1.60 - -1.64$ obtained here agree well with those found by Izotov et al. (2001a), but differ significantly from the value obtained by Pagel et al. (1992). For Tol 1214–277, Pagel et al. (1992) derived a higher value, $\log \text{N/O} = -1.46 \pm 0.06$, while, for Tol 65, they found $\log \text{N/O} = -1.81 \pm 0.15$, lower than the mean for the most metal-deficient BCDs (Izotov & Thuan 1999). Our new determination of the N/O abundance ratio in these two BCDs supports the finding by Thuan et al. (1995) and Izotov & Thuan (1999) that $\log \text{N/O}$ for BCDs with $12 + \log \text{O/H} \lesssim 7.60$ lies in a narrow range, with a mean value of -1.60 .

In Fig. 7 we compare several heavy element-to-oxygen abundance ratios determined from the high- and low-resolution spectra for Tol 1214–277 (filled stars) and Tol 65 (filled squares) with those derived for a sample of 93 BCDs by Izotov & Thuan (1999, 2004), Lipovetsky et al. (1999) and Guseva et al. (2003) (open circles). The heavy element abundance ratios in Tol 1214–277 and Tol 65 are in general agreement with those derived for other very low-metallicity BCDs.

Note the increasing trend of [O/Fe] with increasing $12 + \log \text{O/H}$ (open symbols in Fig. 7f). The relatively low [O/Fe] in Tol 1214–277 and Tol 65 (filled symbols in Fig. 7f) further supports that trend. Such a trend can be explained by a larger Fe depletion onto dust in galaxies with larger oxygen abundance.

Table 2. Corrected fluxes and equivalent widths of the emission lines in the high-resolution spectra of the brightest H II regions in Tol 1214–277 (slit #3) and Tol 65 (slit #6).

λ_0 (Å) Ion	Tol 1214–277		Tol 65			
	region 1		regions 1+2		regions 3+4	
	$I(\lambda)/I(\text{H}\beta)$	EW (Å)	$I(\lambda)/I(\text{H}\beta)$	EW (Å)	$I(\lambda)/I(\text{H}\beta)$	EW (Å)
3704 H16	0.0153 ±0.0018	2.0 ±0.2
3712 H15	0.0160 ±0.0017	2.2 ±0.1
3727 [O II]	0.3584 ±0.0061	47.8 ±0.4	0.5561 ±0.0092	97.8 ±0.4	0.7865 ±0.0177	37.2 ±1.3
3750 H12	0.0328 ±0.0018	5.0 ±0.2	0.0574 ±0.0027	5.0 ±0.2	0.0454 ±0.0298	0.8 ±0.6
3770 H11	0.0419 ±0.0018	6.2 ±0.2	0.0660 ±0.0026	6.1 ±0.2	0.0514 ±0.0262	1.1 ±0.6
3798 H10	0.0590 ±0.0020	8.9 ±0.2	0.0797 ±0.0025	8.2 ±0.2	0.0675 ±0.0201	1.9 ±0.6
3820 He I	0.0132 ±0.0015	2.0 ±0.2	0.0102 ±0.0012	2.0 ±0.2
3835 H9	0.0639 ±0.0020	9.9 ±0.2	0.0946 ±0.0025	11.5 ±0.2	0.0749 ±0.0166	2.1 ±0.6
3868 [Ne III]	0.3739 ±0.0062	57.5 ±0.4	0.2816 ±0.0047	48.8 ±0.3	0.2932 ±0.0088	12.8 ±0.7
3889 H8 + He I	0.2182 ±0.0040	35.1 ±0.3	0.2125 ±0.0039	35.5 ±0.3	0.2058 ±0.0147	8.4 ±0.6
3968 [Ne III] + H7	0.3192 ±0.0054	54.2 ±0.4	0.2790 ±0.0049	42.0 ±0.3	0.2553 ±0.0155	10.3 ±0.6
4026 He I	0.0196 ±0.0010	3.4 ±0.2	0.0158 ±0.0010	2.9 ±0.2	0.0132 ±0.0053	0.6 ±0.4
4068 [S II]	0.0051 ±0.0010	0.9 ±0.2	0.0095 ±0.0010	1.6 ±0.2
4101 H δ	0.2814 ±0.0047	52.6 ±0.4	0.2719 ±0.0046	48.8 ±0.3	0.2691 ±0.0134	12.7 ±0.6
4227 [Fe V]	0.0068 ±0.0008	1.4 ±0.2
4340 H γ	0.4981 ±0.0078	111.5 ±0.6	0.4661 ±0.0073	96.8 ±0.5	0.4714 ±0.0134	27.3 ±0.7
4363 [O III]	0.1775 ±0.0031	40.5 ±0.4	0.0975 ±0.0020	22.7 ±0.3	0.0941 ±0.0044	5.5 ±0.6
4389 He I	0.0049 ±0.0009	1.2 ±0.2	0.0036 ±0.0009	1.0 ±0.2
4471 He I	0.0364 ±0.0011	9.2 ±0.3	0.0352 ±0.0011	8.7 ±0.2	0.0312 ±0.0034	2.0 ±0.4
4658 [Fe III]	0.0039 ±0.0008	1.1 ±0.2	0.0052 ±0.0007	1.4 ±0.2	0.0072 ±0.0027	0.5 ±0.4
4686 He II	0.0531 ±0.0013	15.2 ±0.3	0.0077 ±0.0009	2.2 ±0.2	0.0233 ±0.0029	1.5 ±0.5
4711 [Ar IV]+He I	0.0294 ±0.0010	8.6 ±0.3	0.0123 ±0.0008	3.4 ±0.2	0.0079 ±0.0034	0.5 ±0.3
4725 [Ne IV]	0.0020 ±0.0004	0.6 ±0.2
4740 [Ar IV]	0.0187 ±0.0009	5.6 ±0.3	0.0064 ±0.0006	1.8 ±0.2	0.0066 ±0.0052	0.5 ±0.3
4861 H β	1.0000 ±0.0149	311.6 ±1.0	1.0000 ±0.0150	267.7 ±0.8	1.0000 ±0.0183	77.0 ±1.0
4922 He I	0.0093 ±0.0008	3.1 ±0.2	0.0093 ±0.0007	2.9 ±0.2
4959 [O III]	1.7625 ±0.0259	570.4 ±1.3	1.2645 ±0.0188	355.7 ±0.9	1.1589 ±0.0190	91.1 ±1.0
4988 [Fe III]	0.0046 ±0.0005	1.4 ±0.2	0.0048 ±0.0005	1.4 ±0.2
5007 [O III]	5.2819 ±0.0770	1696.0 ±2.2	3.7565 ±0.0555	1054.2 ±1.4	3.4617 ±0.0548	279.0 ±1.6
5146 [Fe VI]	0.0015 ±0.0006	0.6 ±0.2
5177 [Fe VI]	0.0008 ±0.0005	0.3 ±0.2
5200 [N I]	0.0010 ±0.0006	0.4 ±0.2	0.0035 ±0.0007	1.3 ±0.2
5271 [Fe III]	0.0014 ±0.0009	0.6 ±0.4	0.0027 ±0.0009	1.0 ±0.3
5411 He II	0.0037 ±0.0006	1.6 ±0.3
5517 [Cl III]	0.0022 ±0.0005	1.0 ±0.3	0.0019 ±0.0004	0.8 ±0.2
5537 [Cl III]	0.0011 ±0.0005	0.5 ±0.2	0.0016 ±0.0004	0.7 ±0.2
5721 [Fe VII]	0.0012 ±0.0005	0.6 ±0.2
5876 He I	0.0927 ±0.0018	50.4 ±0.6	0.1043 ±0.0019	48.5 ±0.5	0.0966 ±0.0035	12.7 ±0.8
6087 [Fe VII]	0.0023 ±0.0006	1.3 ±0.3
6300 [O I]	0.0080 ±0.0005	5.1 ±0.3	0.0178 ±0.0006	10.1 ±0.3	0.0190 ±0.0026	2.9 ±0.5
6312 [S III]	0.0076 ±0.0005	4.8 ±0.3	0.0114 ±0.0005	6.6 ±0.3	0.0149 ±0.0018	2.3 ±0.5
6363 [O I]	0.0032 ±0.0005	2.0 ±0.3	0.0062 ±0.0006	3.7 ±0.7
6548 [N II]	0.0035 ±0.0005	1.8 ±0.3	0.0061 ±0.0005	2.3 ±0.2
6563 H α	2.7389 ±0.0435	1798.1 ±3.3	2.7667 ±0.0444	1601.8 ±2.5	2.6651 ±0.0458	422.4 ±2.5
6583 [N II]	0.0094 ±0.0006	4.7 ±0.3	0.0171 ±0.0006	9.3 ±0.3	0.0214 ±0.0018	4.1 ±0.7
6678 He I	0.0249 ±0.0008	18.6 ±0.5	0.0269 ±0.0007	17.4 ±0.4	0.0256 ±0.0017	4.2 ±0.7
6717 [S II]	0.0192 ±0.0006	14.4 ±0.5	0.0503 ±0.0011	32.9 ±0.5	0.0646 ±0.0022	10.8 ±0.8
6731 [S II]	0.0159 ±0.0006	12.0 ±0.4	0.0402 ±0.0010	26.3 ±0.4	0.0439 ±0.0019	7.4 ±0.8
7065 He I	0.0256 ±0.0008	22.5 ±0.6	0.0296 ±0.0008	23.0 ±0.5	0.0238 ±0.0018	4.6 ±0.9
7135 [Ar III]	0.0215 ±0.0007	19.0 ±0.6	0.0281 ±0.0008	23.3 ±0.5	0.0315 ±0.0020	6.6 ±0.9
7281 He I	0.0050 ±0.0005	4.6 ±0.4	0.0066 ±0.0005	6.1 ±0.5	0.0044 ±0.0017	1.0 ±0.7
7320 [O II]	0.0051 ±0.0005	4.7 ±0.4	0.0115 ±0.0005	11.2 ±0.4	0.0146 ±0.0017	3.2 ±0.9
7330 [O II]	0.0045 ±0.0004	4.2 ±0.4	0.0099 ±0.0005	10.0 ±0.4	0.0124 ±0.0015	2.7 ±0.9
$C(\text{H}\beta)$ dex	0.105 ±0.019		0.065 ±0.019		0.000 ±0.020	
$F(\text{H}\beta)^a$	1.62 ±0.01		1.64 ±0.01		0.38 ±0.01	
$EW(\text{abs})$ Å	0.0 ±0.2		5.9 ±0.2		1.3 ±0.6	

^ain units 10^{-14} erg s^{-1} cm^{-2} .

Table 3. Corrected fluxes and equivalent widths of the emission lines in the low-resolution spectra of the brightest H II regions in Tol 1214–277 (slit #1).

λ_0 (Å) Ion	Region 1				Region 2			
	1999		2000		1999		2000	
	$I(\lambda)/I(H\beta)$	EW^a	$I(\lambda)/I(H\beta)$	EW^a	$I(\lambda)/I(H\beta)$	EW^a	$I(\lambda)/I(H\beta)$	EW^a
3727 [O II]	0.237±0.007	40.6	0.285±0.007	42.6	1.928±0.342	53.8	1.361±0.209	40.8
3750 H12	0.044±0.009	4.0	0.034±0.006	4.3
3770 H11	0.050±0.008	5.1	0.049±0.006	6.7
3798 H10	0.064±0.007	7.5	0.067±0.006	9.5
3820 He I	0.009±0.003	1.5	0.009±0.002	1.4
3835 H9	0.068±0.003	8.2	0.061±0.005	8.7
3868 [Ne III]	0.321±0.006	57.4	0.357±0.007	56.4
3889 H8 + He I	0.208±0.006	35.3	0.216±0.006	34.0
3968 [Ne III] + H7	0.297±0.007	53.6	0.317±0.007	53.5
4026 He I	0.017±0.002	3.4	0.017±0.002	3.1
4068 [S II]	0.006±0.001	1.3	0.009±0.002	1.6
4101 H δ	0.263±0.006	52.1	0.277±0.006	53.1
4227 [Fe V]	0.010±0.002	2.3	0.009±0.002	1.8
4340 H γ	0.476±0.008	107.5	0.488±0.008	110.0	0.418±0.093	7.3	0.482±0.081	15.6
4363 [O III]	0.171±0.003	40.6	0.172±0.003	39.8
4389 He I	0.005±0.001	1.3	0.005±0.001	1.2
4471 He I	0.033±0.002	8.3	0.037±0.001	10.0
4658 [Fe III]	0.004±0.001	1.1
4686 He II	0.057±0.002	16.6	0.053±0.001	15.0
4711 [Ar IV]+He I	0.033±0.001	9.5	0.032±0.001	9.3
4740 [Ar IV]	0.023±0.001	6.7	0.020±0.001	6.0
4861 H β	1.000±0.015	320.2	1.000±0.015	315.3	1.000±0.086	32.6	1.000±0.068	50.2
4922 He I	0.011±0.001	3.7	0.008±0.001	2.6
4959 [O III]	1.710±0.025	580.1	1.736±0.025	571.7	0.493±0.052	20.9	0.380±0.035	16.4
5007 [O III]	5.127±0.075	1794.0	5.220±0.075	1789.0	1.447±0.102	63.7	1.314±0.073	59.7
5200 [N I]	0.003±0.001	1.4
5411 He II	0.004±0.001	1.6	0.004±0.001	1.7
5876 He I	0.090±0.002	50.5	0.095±0.002	49.9
6300 [O I]	0.010±0.001	6.5	0.009±0.001	5.7
6363 [O I]	0.003±0.001	2.2	0.003±0.001	2.0
6563 H α	2.401±0.038	1799.0	2.739±0.043	1807.0	2.879±0.196	227.2	2.878±0.153	268.1
6583 [N II]	0.007±0.001	3.7	0.010±0.001	5.7
6678 He I	0.025±0.001	21.4	0.026±0.001	19.3
6717 [S II]	0.016±0.001	13.8	0.018±0.001	13.2
6731 [S II]	0.014±0.001	12.3	0.015±0.001	10.6
7065 He I	0.027±0.001	22.6	0.026±0.001	22.4
7135 [Ar III]	0.022±0.001	20.1	0.022±0.001	19.1
$C(H\beta)$ dex	0.085±0.019		0.065±0.019		0.000±0.073		0.030±0.063	
$F(H\beta)^b$	1.69±0.01		1.62±0.01		0.02±0.01		0.02±0.01	
$EW(ABS)$ Å	3.5±0.7		0.9±0.6		3.9±0.6		0.1±1.0	

^ain Å.^bin units 10^{-14} erg s $^{-1}$ cm $^{-2}$.

3.2.2. Low-resolution spectra

The heavy element abundances obtained from the low-resolution spectra, together with the adopted electron temperatures, electron number densities and ionization correction factors, are shown in Table 6 for region 1 in Tol 1214–277, observed in 1999 and 2000 at slit position #1, and regions 1 to 4 in Tol 65, observed in 1999 at slit position #4. The oxygen abundance for region 1 in Tol 1214–277 derived from the low-resolution observations is very similar to that obtained from the high-resolution ob-

servations (Table 5). The other heavy element abundances are also in good agreement. The oxygen abundance for regions 1 – 4 in Tol 65 derived from the low-resolution spectra is slightly lower than that found for regions 1+2 and 3+4 from the high-resolution spectra. The agreement between other heavy element abundances is good.

3.3. Helium abundance

He emission-line strengths in the high- and low-resolution spectra of region 1 in Tol 1214–277 and regions 1–4 in Tol

Table 4. Corrected fluxes and equivalent widths of the emission lines in the low-resolution spectra of the brightest H II regions in Tol 65 (slit #4).

$\lambda_0(\text{\AA})$ Ion	Region 1		Region 2		Region 3		Region 4	
	$I(\lambda)/I(\text{H}\beta)$	EW^a	$I(\lambda)/I(\text{H}\beta)$	EW^a	$I(\lambda)/I(\text{H}\beta)$	EW^a	$I(\lambda)/I(\text{H}\beta)$	EW^a
3727 [O II]	0.449±0.010	91.6	0.684±0.021	78.2	0.739±0.080	18.4	0.614±0.030	33.7
3750 H12	0.030±0.005	6.0	0.019±0.012	2.2
3770 H11	0.038±0.005	7.7	0.022±0.013	2.5
3798 H10	0.044±0.005	8.5	0.037±0.013	4.3
3835 H9	0.062±0.005	12.1	0.059±0.014	6.5
3868 [Ne III]	0.313±0.006	60.7	0.250±0.010	26.9	0.278±0.046	5.4	0.304±0.015	14.0
3889 H8 + He I	0.180±0.006	33.8	0.177±0.014	19.0	0.189±0.084	1.9	0.153±0.016	7.1
3968 [Ne III] + H7	0.275±0.007	51.0	0.237±0.013	25.7	0.226±0.063	2.5	0.249±0.017	11.8
4026 He I	0.016±0.002	3.0
4068 [S II]	0.009±0.001	1.8
4101 H δ	0.253±0.006	51.6	0.247±0.012	29.1	0.243±0.052	3.6	0.229±0.014	11.9
4340 H γ	0.493±0.009	111.6	0.485±0.013	65.2	0.485±0.036	10.1	0.511±0.014	32.1
4363 [O III]	0.122±0.003	28.0	0.094±0.005	12.8	0.097±0.029	2.3	0.119±0.008	7.4
4389 He I	0.005±0.002	1.3
4471 He I	0.036±0.001	9.1	0.038±0.004	5.9	0.022±0.006	1.5
4658 [Fe III]	0.004±0.001	1.1
4686 He II	0.006±0.001	1.8	0.034±0.005	2.6
4711 [Ar IV]+He I	0.014±0.001	4.1	0.012±0.002	2.1
4740 [Ar IV]	0.007±0.001	2.1
4861 H β	1.000±0.015	310.9	1.000±0.017	191.3	1.000±0.032	33.9	1.000±0.019	89.3
4922 He I	0.007±0.001	2.3
4959 [O III]	1.341±0.020	430.5	1.095±0.018	217.5	1.034±0.030	37.8	1.284±0.022	122.4
5007 [O III]	4.043±0.059	1371.0	3.277±0.051	659.0	3.136±0.076	119.4	3.810±0.062	363.3
5200 [N I]	0.005±0.001	1.8
5271 [Fe III]	0.003±0.001	1.4
5517 [Cl III]	0.003±0.001	1.3
5537 [Cl III]	0.002±0.001	1.0
5876 He I	0.104±0.002	54.8	0.099±0.003	34.2	0.092±0.011	5.5	0.096±0.004	14.8
6300 [O I]	0.020±0.001	12.7	0.024±0.002	9.4
6363 [O I]	0.006±0.001	12.7
6563 H α	2.749±0.043	1807.0	2.748±0.046	1173.0	2.451±0.065	194.9	2.526±0.045	560.8
6583 [N II]	0.013±0.001	7.0	0.024±0.004	12.1
6678 He I	0.028±0.001	19.6	0.029±0.003	13.0	0.031±0.004	7.5
6717 [S II]	0.043±0.001	30.5	0.072±0.002	31.2	0.071±0.009	6.1
6731 [S II]	0.033±0.001	23.8	0.044±0.002	19.4	0.042±0.007	3.7
7065 He I	0.034±0.001	27.7	0.027±0.002	14.9	0.027±0.004	7.7
7135 [Ar III]	0.028±0.001	24.2	0.034±0.003	19.0	0.033±0.004	9.5
7281 He I	0.006±0.001	5.1	0.008±0.003	4.9
$C(\text{H}\beta)$ dex	0.045±0.019		0.000±0.020		0.000±0.030		0.000±0.021	
$F(\text{H}\beta)^b$	1.79±0.01		0.54±0.01		0.12±0.01		0.30±0.01	
$EW(\text{abs})$ \AA	0.3±0.8		0.0±1.2		1.8±0.4		0.0±0.5	

^ain \AA .^bin units 10^{-14} erg s^{-1} cm^{-2} .

65 are converted to singly ionized helium $y^+ \equiv \text{He}^+/\text{H}^+$ and doubly ionized helium $y^{+2} \equiv \text{He}^{+2}/\text{H}^+$ abundances, using the theoretical He I recombination line emissivities by Smits (1996).

The helium mass fraction was calculated as

$$Y = \frac{4y[1 - 20(\text{O}/\text{H})]}{1 + 4y}, \quad (3)$$

where $y = y^+ + y^{+2}$ is the number density of helium relative to hydrogen (Pagel et al. 1992).

The main mechanisms causing deviations of the observed He I emission line fluxes from their theoretical values are collisional and fluorescent enhancement. In order to correct for these effects, we have adopted the procedure, discussed in more detail in Izotov et al. (1994, 1997a) and Izotov & Thuan (1998). The singly ionized helium abundance y^+ and He mass fraction Y is obtained for each of the three He I $\lambda 4471$, $\lambda 5876$ and $\lambda 6678$ lines. We then derive the weighted mean y^+ of these three determinations, the weight of each line being scaled to its intensity. The obtained ionic and total He abundances (y^+ , y^{+2} , y) and

Table 5. Physical conditions and element abundances derived from the high-resolution spectra of the brightest H II regions of Tol 1214–277 (slit #3) and Tol 65 (slit #6).

Value	Tol 1214–277		Tol 65	
	region 1	regions 1+2	regions 3+4	
$T_e(\text{O III})(\text{K})$	19970±250	17270±210	17720±460	
$T_e(\text{O II})(\text{K})$	15680±180	14750±170	14920±370	
$T_e(\text{S III})(\text{K})$	18280±210	16030±170	16400±390	
$N_e(\text{S II})(\text{cm}^{-3})$	250±90	190±50	10±10	
$N_e(\text{He II})(\text{cm}^{-3})$	70±40	260±50	20±10	
$\tau(\lambda 3889)$	0.0	0.0	0.0	
$\text{O}^+/\text{H}^+(\times 10^5)$	0.280±0.009	0.517±0.018	0.692±0.048	
$\text{O}^{+2}/\text{H}^+(\times 10^5)$	3.041±0.093	2.943±0.093	2.560±0.163	
$\text{O}^{+3}/\text{H}^+(\times 10^6)$	2.136±0.105	0.305±0.036	0.904±0.136	
$\text{O}/\text{H}(\times 10^5)$	3.534±0.094	3.490±0.095	3.343±0.170	
$12 + \log(\text{O}/\text{H})$	7.548±0.012	7.543±0.012	7.524±0.022	
$\text{N}^+/\text{H}^+(\times 10^7)$	0.644±0.032	1.312±0.046	1.603±0.127	
ICF(N) ^a	12.6	6.76	4.83	
$\log(\text{N}/\text{O})$	-1.638±0.025	-1.595±0.019	-1.635±0.041	
$\text{Ne}^{+2}/\text{H}^+(\times 10^5)$	0.436±0.014	0.467±0.015	0.455±0.031	
ICF(Ne) ^a	1.16	1.19	1.31	
$\log(\text{Ne}/\text{O})$	-0.843±0.018	-0.800±0.019	-0.750±0.037	
$\text{S}^+/\text{H}^+(\times 10^7)$	0.330±0.011	0.937±0.023	1.079±0.049	
$\text{S}^{+2}/\text{H}^+(\times 10^7)$	2.236±0.164	4.772±0.257	5.850±0.794	
ICF(S) ^a	2.91	1.88	1.56	
$\log(\text{S}/\text{O})$	-1.676±0.030	-1.513±0.023	-1.490±0.055	
$\text{Cl}^{+2}/\text{H}^+(\times 10^8)$	0.505±0.115	0.691±0.121	...	
ICF(Cl) ^a	1.85	1.77	...	
$\log(\text{Cl}/\text{O})$	-3.578±0.100	-3.455±0.077	...	
$\text{Ar}^{+2}/\text{H}^+(\times 10^7)$	0.567±0.020	0.908±0.028	0.979±0.068	
$\text{Ar}^{+3}/\text{H}^+(\times 10^7)$	1.469±0.077	0.671±0.067	0.657±0.526	
ICF(Ar) ^a	1.01	1.02	1.04	
$\log(\text{Ar}/\text{O})$	-2.237±0.021	-2.337±0.023	-2.295±0.143	
$\text{Fe}^{+2}/\text{H}^+(\times 10^7)$	0.661±0.129	1.027±0.149	1.382±0.517	
ICF(Fe) ^a	15.8	8.44	6.04	
$\log(\text{Fe}/\text{O})$	-1.530±0.086	-1.605±0.064	-1.603±0.164	
[O/Fe]	0.110±0.086	0.185±0.064	0.183±0.164	
$\text{He}^+/\text{H}^+(\lambda 4471)$	0.0777±0.0027	0.0717±0.0023	0.0671±0.0072	
$\text{He}^+/\text{H}^+(\lambda 5876)$	0.0769±0.0021	0.0798±0.0018	0.0803±0.0029	
$\text{He}^+/\text{H}^+(\lambda 6678)$	0.0755±0.0024	0.0774±0.0021	0.0760±0.0051	
$\text{He}^+/\text{H}^+(\text{mean})$	0.0767±0.0014	0.0768±0.0012	0.0779±0.0024	
$\text{He}^{+2}/\text{H}^+(\lambda 4686)$	0.0049±0.0001	0.0007±0.0001	0.0021±0.0003	
He/H	0.0816±0.0014	0.0775±0.0012	0.0800±0.0024	
Y	0.2459±0.0043	0.2365±0.0037	0.2423±0.0075	

^aICF is the ionization correction factor.

mass fractions (Y) in Tol 1214–277 and Tol 65 are shown in Tables 5 and 6. In general, they are consistent with the He abundances found by Izotov et al. (2001a) from the Keck observations of both BCDs. They are also consistent with the primordial helium mass fraction $Y_p = 0.244 - 0.245$ obtained by Izotov & Thuan (1998) and Izotov et

al. (1999). An exception is the He mass fraction Y determined from the high-resolution spectrum of regions 1+2 in Tol 65, which is lower (Table 5). However, at the 95% confidence level, it is consistent with other determinations of Y in Tol 65.

Table 6. Physical conditions and element abundances derived from the low-resolution spectra of the brightest H II regions of Tol 1214–277 (slit #1) and Tol 65 (slit #4).

Value	Tol 1214–277 (region 1)		Tol 65			
	1999	2000	region 1	region 2	region 3	region 4
$T_e(\text{O III})(\text{K})$	19850±260	19760±250	18740±250	18240±500	19030±3260	19100±740
$T_e(\text{O II})(\text{K})$	15640±190	15650±180	15300±190	15110±390	15390±2460	15410±560
$T_e(\text{S III})(\text{K})$	18170±220	18100±210	17260±210	16840±420	17500±2700	17550±610
$N_e(\text{S II})(\text{cm}^{-3})$	410±150	220±90	140±60	10±10	10±10	10±10
$N_e(\text{He II})(\text{cm}^{-3})$	10±1	70±1	220±50	10±1	...	10±3
$\tau(\lambda 3889)$	0.3	0.0	0.2	0.2	...	0.2
$\text{O}^+/\text{H}^+(\times 10^5)$	0.189±0.008	0.224±0.009	0.372±0.014	0.579±0.043	0.594±0.250	0.491±0.051
$\text{O}^{+2}/\text{H}^+(\times 10^5)$	2.989±0.096	3.067±0.095	2.645±0.087	2.276±0.150	1.985±0.784	2.407±0.217
$\text{O}^{+3}/\text{H}^+(\times 10^6)$	2.181±0.119	2.019±0.100	0.214±0.031	0.947±0.201
$\text{O}/\text{H}(\times 10^5)$	3.397±0.097	3.494±0.096	3.039±0.088	2.855±0.156	2.578±0.823	2.993±0.224
$12 + \log(\text{O}/\text{H})$	7.531±0.012	7.543±0.012	7.483±0.013	7.456±0.024	7.411±0.139	7.476±0.032
$\text{N}^+/\text{H}^+(\times 10^7)$	0.497±0.038	0.672±0.048	0.894±0.040	1.786±0.213
ICF(N) ^a	17.9	15.6	8.16	4.93
$\log(\text{N}/\text{O})$	-1.581±0.035	-1.524±0.033	-1.620±0.023	-1.511±0.057
$\text{Ne}^{+2}/\text{H}^+(\times 10^5)$	0.380±0.013	0.426±0.014	0.424±0.015	0.361±0.026	0.362±0.147	0.393±0.038
ICF(Ne) ^a	1.14	1.14	1.15	1.25	1.30	1.24
$\log(\text{Ne}/\text{O})$	-0.895±0.019	-0.857±0.019	-0.796±0.020	-0.800±0.040	-0.739±0.225	-0.787±0.053
$\text{Cl}^{+2}/\text{H}^+(\times 10^8)$	0.857±0.144
ICF(Cl) ^a	1.91
$\log(\text{Cl}/\text{O})$	-3.270±0.074
$\text{Ar}^{+2}/\text{H}^+(\times 10^7)$	0.595±0.027	0.583±0.020	0.798±0.029	1.007±0.081	...	0.933±0.116
$\text{Ar}^{+3}/\text{H}^+(\times 10^7)$	1.789±0.109	1.618±0.086	0.622±0.095
ICF(Ar) ^a	1.01	1.01	1.01	1.89	...	2.11
$\log(\text{Ar}/\text{O})$	-2.152±0.023	-2.198±0.021	-2.325±0.033	-2.176±0.042	...	-2.182±0.063
$\text{Fe}^{+2}/\text{H}^+(\times 10^7)$...	0.692±0.012	0.728±0.184
ICF(Fe) ^a	...	19.5	10.2
$\log(\text{Fe}/\text{O})$...	-1.381±0.073	-1.639±0.110
[O/Fe]	...	-0.006±0.074	0.192±0.111
$\text{He}^+/\text{H}^+(\lambda 4471)$	0.0726±0.0032	0.0783±0.0031	0.0742±0.0029	0.0816±0.0086	...	0.0481±0.0119
$\text{He}^+/\text{H}^+(\lambda 5876)$	0.0768±0.0015	0.0788±0.0014	0.0805±0.0015	0.0827±0.0026	...	0.0810±0.0035
$\text{He}^+/\text{H}^+(\lambda 6678)$	0.0768±0.0027	0.0788±0.0024	0.0806±0.0026	0.0854±0.0076	...	0.0943±0.0122
$\text{He}^+/\text{H}^+(\text{mean})$	0.0762±0.0012	0.0787±0.0011	0.0795±0.0012	0.0829±0.0023	...	0.0795±0.0033
$\text{He}^{+2}/\text{H}^+(\lambda 4686)$	0.0053±0.0001	0.0049±0.0001	0.0006±0.0001	0.0031±0.0005
He/H	0.0815±0.0012	0.0836±0.0012	0.0801±0.0012	0.0829±0.0023	...	0.0826±0.0033
Y	0.2457±0.0038	0.2504±0.0036	0.2425±0.0036	0.2488±0.0072	...	0.2482±0.0102

^aICF is the ionization correction factor.

4. High-ionization emission lines in Tol 1214–277

Several emission lines of the high-ionization ions are detected in the high-resolution spectrum of Tol 1214–277 (Table 2, Fig. 2). The presence of these lines implies the existence of a substantial ionizing radiation field with $\lambda \lesssim 228\text{\AA}$ (equivalent to photon energies $\gtrsim 4$ Ryd) in the brightest H II region 1. In addition to confirming the findings of previous papers such as [Fe V] $\lambda 4227$ and strong He II $\lambda 4686$ emission, we detect here also emission lines of Ne IV (the ionization potential of Ne^{+3} is 4.664 Ryd), Fe VI (the ionization potential of Fe^{+5} is 5.513 Ryd) and Fe

VII (the ionization potential of Fe^{+6} is 7.281 Ryd). The large difference in the ionization potentials of these different ions allows in principle to determine the slope of the hard radiation spectrum.

To constrain the nature of the hard ionizing radiation in Tol 1214–277, we compare our observations with a spherically symmetric ionization-bounded H II region model calculated with the CLOUDY94 code (Ferland 1996; Ferland et al. 1998) for the physical conditions of the brightest H II region. The input parameters are the element abundances from Table 5 and the flux of ionizing photons Q_{H} (in s^{-1}) at $\lambda 912\text{\AA}$ as determined from the H β

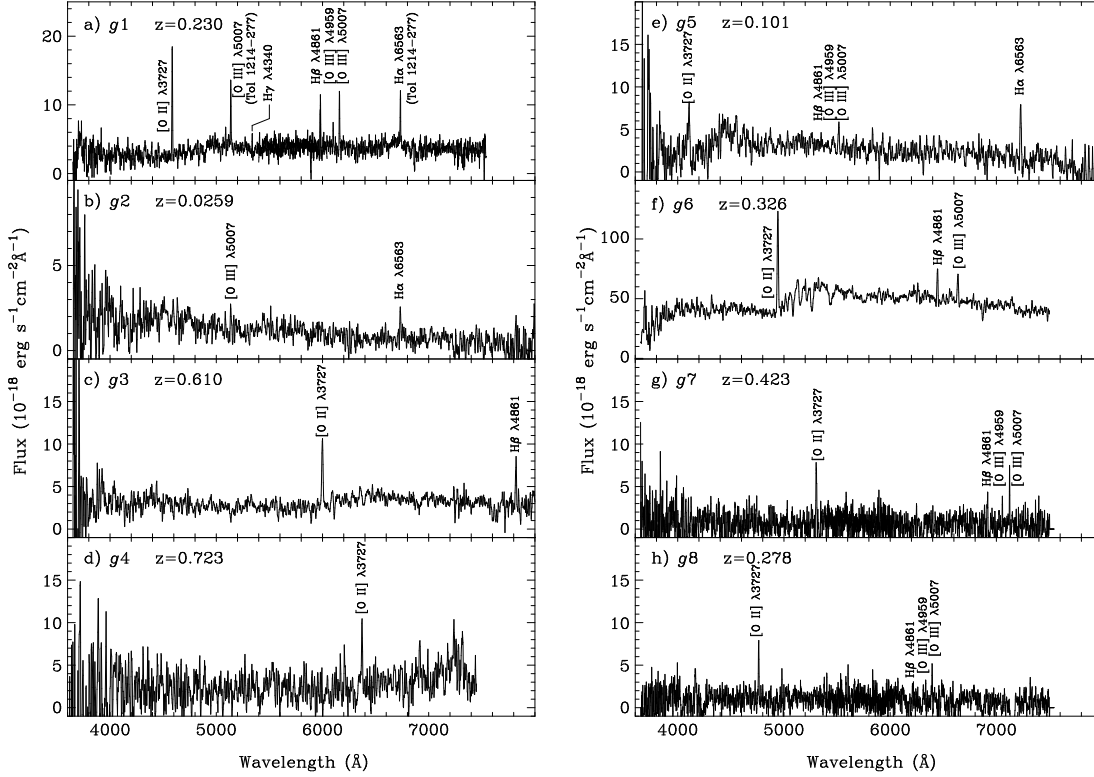


Fig. 8. Spectra of the emission-line galaxies in the fields of Tol 1214–277 (left panel) and Tol 65 (right panel). The emission lines are labeled. The spectrum of the galaxy *g1* is contaminated by the emission lines of Tol 1214–277. All galaxies except for the galaxy *g2* (b) are background galaxies. The galaxies Tol 1214–277 and *g2* have the same redshift and are likely physically related.

Table 7. Coordinates of the emission-line galaxies in the fields of Tol 1214–277 and Tol 65.

Name	α (J2000.0)	δ (J2000.0)
Tol 1214–277 ^a	12 ^h 17 ^m 17 ^s .1	–28°02′33″
<i>g1</i>	12 17 17.0	–28 02 27
<i>g2</i>	12 17 15.5	–28 02 49
<i>g3</i>	12 17 14.0	–28 02 53
<i>g4</i>	12 17 25.0	–28 00 17
Tol 65 ^a	12 25 46.9	–36 14 01
<i>g5</i>	12 25 45.6	–36 14 13
<i>g6</i>	12 25 51.5	–36 13 12
<i>g7</i>	12 25 59.1	–36 16 05
<i>g8</i>	12 25 42.9	–36 13 24

^a Coordinates of the brightest region 1.

emission line luminosity $L(\text{H}\beta)$. Because the spectrum of Tol 1214–277 is not properly flux-calibrated, we adopt $\log Q_{\text{H}} = 52.7$ from Izotov et al. (2004). As source of ionizing radiation, we chose to use the hottest CoStar stellar atmosphere model F1, with a heavy element mass fraction $Z = 0.004$ ($Z_{\odot}/5$) (the lowest Z available for the CoStar models) and an effective temperature $T_{\text{eff}} = 54000\text{K}$ (Schaerer & de Koter 1997). This model predicts harder radiation for $\lambda \lesssim 228\text{\AA}$ as compared to Kurucz (1979)’s stellar atmosphere models.

The model predicts the He II $\lambda 4686$ flux and the [Ne IV] $\lambda 4725$ /[Ne III] $\lambda 3868$ flux ratio to be respectively ~ 50 and ~ 200 times lower than the ones observed. As for the high-ionization iron lines, the model predicts flux ratios [Fe VI] $\lambda 5146$ /[Fe III] $\lambda 4658$ and [Fe VII] $\lambda 6087$ /[Fe III] $\lambda 4658$ respectively ~ 500 and $\sim 10^5$ times lower than the ones observed. The disagreement between predicted and observed emission line fluxes increases for ions of higher ionization degree. This implies that the spectrum of hard radiation for energies > 4 Ryd in Tol 1214–277 increases more steeply at higher energies, as compared to the predictions of the CoStar models. The disagreement between the observed and predicted fluxes and flux ratios is not likely to diminish significantly if models with the lower Tol 1214–277 ionized gas metallicity are used, because $\log Q_{\text{He}^+}/Q_{\text{H}}$ is nearly constant for main-sequence stellar population models with $Z \gtrsim Z_{\odot}/50$ (Schaerer 2002, 2003). Here Q_{He^+} is the flux of ionizing photons with $\lambda \leq 228\text{\AA}$ (≥ 4 Ryd). In principle, it is possible to reproduce the observed He II $\lambda 4686$ and [Ne IV] $\lambda 4725$ emission line fluxes by assuming that the massive stars in the ionizing cluster of Tol 1214–277 have the very low metallicity, of $Z \lesssim 10^{-7}$. However, the predicted equivalent widths of H β and Ly α emission lines in such models (Schaerer 2002, 2003) are several times larger than those observed (Table 2; Thuan & Izotov 1997). Furthermore, these models cannot reproduce the observed fluxes of [Fe VI] and [Fe VII] emission

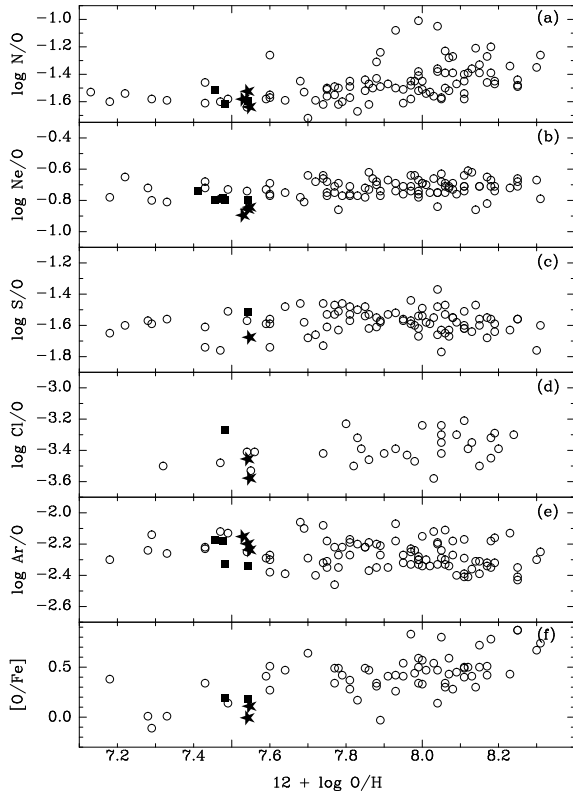


Fig. 7. Abundance ratios in Tol 1214–277 (stars) and Tol 65 (squares) as a function of oxygen abundance $12 + \log O/H$: (a) N/O; (b) Ne/O; (c) S/O; (d) Cl/O; (e) Ar/O; (f) $[O/Fe] \equiv \log(O/Fe) - \log(O/Fe)_{\odot}$, where $\log(O/Fe)_{\odot} = -1.42$ (Anders & Grevesse 1989). Open circles are the data from Izotov & Thuan (1999, 2004), Lipovetsky et al. (1999) and Guseva et al. (2003).

lines. This suggests that an additional compact source of X-ray emission is likely to be present in the brightest H II region of Tol 1214–277. Fast shocks with velocities of $\sim 400 - 500 \text{ km s}^{-1}$ (Dopita & Sutherland 1996) would reproduce both the He II and Fe VII emission. High mass X-ray binary systems are also possible sources of X-ray emission.

We now estimate the X-ray luminosity needed to account for the high-ionization lines. Using the value of Q_H derived from the observations, we scale the spectral energy distribution of stellar atmosphere model F1 to fit the line fluxes of the low-ionization ions. Adopting a multiplicative factor of 10^5 , required to bring the ionizing radiation fluxes at $\lambda \sim 100 \text{ \AA}$ ($\sim 7 - 8 \text{ Ryd}$) of the CoStar models to the level of the observed fluxes of the Fe VII ions, we find that the X-ray luminosity of the ionizing cluster should be as high as $10^{39} - 10^{40} \text{ erg s}^{-1}$, in agreement with the conclusions of Izotov et al. (2004) who discovered unusually strong $[\text{Ne V}] \lambda 3426$ emission in the spectrum of Tol 1214–277. We note also that Thuan et al. (2004) using *Chandra* observations have found in the two most metal-deficient BCDs known, I Zw 18 and SBS 0335–052, X-ray point sources with $0.5 - 10 \text{ Kev}$ luminosities in the range $1.3 -$

Table 8. Parameters of the emission lines in the spectra of galaxies in the fields of Tol 1214–277 and Tol 65.

$\lambda_0(\text{\AA})$	Ion	$\lambda_{obs}(\text{\AA})$	$F(\lambda)^a$	$EW(\text{\AA})$	z^b
<i>g1 (slit #3)</i>					
3727	[O II]	4585.2 ± 0.1	12.5 ± 0.7	52 ± 3	0.2303
4340	H γ	5338.2 ± 0.3	1.7 ± 0.3	7 ± 1	0.2299
4861	H β	5979.4 ± 0.2	4.3 ± 0.5	18 ± 2	0.2299
4959	[O III]	6100.5 ± 0.7	2.0 ± 0.8	6 ± 2	0.2302
5007	[O III]	6159.6 ± 0.4	5.1 ± 1.1	15 ± 3	0.2302
<i>g2 (slit #2)</i>					
5007	[O III]	5137.0 ± 0.9	1.9 ± 0.5	20 ± 5	0.0260
6563	H α	6732.5 ± 0.8	2.3 ± 0.5	43 ± 10	0.0259
<i>g3 (slit #2)</i>					
3727	[O II]	5999.0 ± 0.4	12.2 ± 1.0	47 ± 4	0.6096
4861	H β	7821.1 ± 0.4	6.7 ± 0.8	26 ± 3	0.6088
<i>g4 (slit #1)</i>					
3727	[O II]	6421.8 ± 1.0	8.4 ± 1.7	34 ± 7	0.7231
<i>g5 (slit #5)</i>					
3727	[O II]	4105.7 ± 1.0	10.6 ± 1.6	51 ± 8	0.1016
4861	H β	5350.1 ± 1.1	1.2 ± 0.6	4 ± 2	0.1005
4959	[O III]	5463.2 ± 2.6	3.3 ± 1.2	13 ± 5	0.1017
5007	[O III]	5515.9 ± 0.9	3.9 ± 0.9	15 ± 4	0.1017
6563	H α	7228.5 ± 0.4	9.9 ± 1.0	118 ± 12	0.1014
<i>g6 (slit #5)</i>					
3727	[O II]	4942.4 ± 0.2	107.7 ± 3.6	27 ± 1	0.3261
4861	H β	6445.4 ± 0.4	34.4 ± 3.2	7 ± 1	0.3258
5007	[O III]	6637.2 ± 0.5	34.5 ± 2.9	7 ± 1	0.3256
<i>g7 (slit #6)</i>					
3727	[O II]	5304.7 ± 0.7	6.0 ± 0.9	65 ± 12	0.4233
4861	H β	6917.4 ± 0.8	1.9 ± 0.6	47 ± 22	0.4229
4959	[O III]	7056.0 ± 0.8	1.6 ± 0.8	50 ± 17	0.4229
5007	[O III]	7124.0 ± 0.4	3.6 ± 0.7	230 ± 17	0.4229
<i>g8 (slit #6)</i>					
3727	[O II]	4762.0 ± 0.5	4.7 ± 0.7	52 ± 9	0.2777
4861	H β	6210.1 ± 1.9	1.0 ± 0.6	18 ± 11	0.2775
4959	[O III]	6334.0 ± 1.5	1.2 ± 0.6	28 ± 14	0.2773
5007	[O III]	6395.2 ± 0.7	2.4 ± 0.8	33 ± 10	0.2773

^ain units $10^{-17} \text{ erg s}^{-1} \text{ cm}^{-2}$.

^b redshift.

$8.5 \times 10^{39} \text{ erg s}^{-1}$, just the range of X-ray luminosities predicted by our scaling argument.

5. Emission-line galaxies in the fields of Tol 1214–277 and Tol 65

One of the aims of this study was the search for emission-line companion galaxies of Tol 1214–277 and Tol 65. For this we use spectroscopic observations with different slit orientations (slits #1 – #6 in Table 1 and Fig. 1), chosen to go through extended sources with irregular morphology and/or blue colour, as seen on deep VLT images of the fields around Tol 1214–277 and Tol 65 (Fricke et al. 2001; Papaderos et al. 1999).

We found in total four emission-line galaxies in the field of Tol 1214–277 and four emission-line galaxies in the field of Tol 65. These galaxies are labeled in Fig. 1, and their equatorial coordinates at epoch J2000.0 are given in Table 7, along with the coordinates of Tol 1214–277 and

Tol 65. Note that the galaxies $g2$ and $g3$ correspond to the galaxies G_2 and G_3 discussed by Fricke et al. (2001), and the galaxy $g5$ corresponds to the galaxy G_1 in Papaderos et al. (1999).

The spectra of the emission-line galaxies in the fields of Tol 1214–277 and Tol 65 are shown respectively in the left and right panels of Fig. 8. In each spectrum, except for that of galaxy $g4$ (Fig. 8d), several emission lines are detected, most often the [O II] $\lambda 3727$, H β $\lambda 4861$, [O III] $\lambda 4959$, $\lambda 5007$ lines. In the spectrum of $g4$, only one emission line is present. We identify the line to be [O II] $\lambda 3727$, as the continuum longward of this emission line increases, as seen in the spectra of several other galaxies in Fig. 8. Note also that the spectrum of $g1$ is contaminated by the emission lines of Tol 1214–277.

In Table 8 we show the rest-frame and observed wavelengths, fluxes and equivalent widths of the lines in the emission-line galaxies, and redshifts, derived for each line. Note that, despite the noisy spectra, the redshifts derived from different emission lines in the same galaxy are in very good agreement.

All emission-line galaxies in the fields of Tol 1214–277 and Tol 65 except for galaxy $g2$, are more distant background galaxies with redshifts ranging from ~ 0.1 to ~ 0.7 . In particular galaxy $g5$, suggested by Papaderos et al. (1999) to be a low-surface-brightness companion galaxy of Tol 65, is in fact a background galaxy.

The only companion galaxy to Tol 1214–277 is $g2$. Its spectrum is characterized by a flux increase to the blue and two weak emission lines, [O III] $\lambda 5007$ and H α , with the same redshift as Tol 1214–277. The projected linear distance between Tol 1214–277 and $g2$ is 14.5 kpc.

Tol 1214–277 is not unique among the most metal-deficient BCDs in having a companion galaxy. Such companions are also seen for other very metal-deficient BCDs such as SBS 0335–052 (Pustilnik et al. 1997) and HS 0822+3542 (Pustilnik et al. 2003) at projected distances of ~ 22 kpc and ~ 11 kpc, respectively. VLA 21 cm observations of SBS 0335–052 (Pustilnik et al. 2001) reveal that the BCD and its companion are embedded in a large cloud of neutral gas implying a common origin. It would be interesting to carry out such H I VLA observations for Tol 1214–277 to check whether the BCD and its companion galaxy are also part of the same system.

6. Conclusions

Our main conclusions from the VLT spectroscopic study of the blue compact dwarf (BCD) galaxies Tol 1214–277 and Tol 65 and the fields around these galaxies may be summarized as follows:

1. The oxygen abundances $12 + \log \text{O}/\text{H}$ in the brightest regions of Tol 1214–277 and Tol 65 derived from high-resolution spectra are, respectively, 7.55 ± 0.01 and 7.54 ± 0.01 , or $\sim Z_{\odot}/24$. These values are in good agreement with previous determinations by Fricke et al. (2001) and Izotov et al. (2001a). The high spectral resolution allows to separate the [N II] $\lambda 6583$ emission line from the strong H α

emission line and reliably determine the nitrogen abundance. We find $\log \text{N}/\text{O} = -1.64 \pm 0.03$ and -1.60 ± 0.02 respectively, in agreement with previous determinations by Izotov et al. (2001a), and consistent with the mean value of $\log \text{N}/\text{O} = -1.60$ obtained by Izotov & Thuan (1999) for very metal-deficient BCDs with $12 + \log \text{O}/\text{H} < 7.6$.

2. The He mass fraction derived for several regions in Tol 1214–277 and Tol 65 is in the range $Y = 0.242 - 0.250$, consistent with the values obtained by Izotov et al. (2001a) for both galaxies, and with the primordial He mass fraction $Y_p = 0.244 - 0.245$ obtained by Izotov & Thuan (1998, 2004) and Izotov et al. (1999). An exception is the He mass fraction $Y = 0.237$ derived for regions 1 + 2 in Tol 65 because of likely contamination by underlying stellar He I absorption. However, at the 95% confidence level, this value is consistent with other determinations of the He abundance in Tol 65.

3. Strong He II $\lambda 4686$ emission, with an intensity as high as 5% of that of the H β emission line, and the high ionization line [Fe V] $\lambda 4227$ are seen in the spectrum of Tol 1214–277, confirming previous findings by Fricke et al. (2001) and Izotov et al. (2001a). Additionally, weak [Ne IV] $\lambda 4725$, [Fe VI] $\lambda 5146$, $\lambda 5177$, [Fe VII] $\lambda 5721$, $\lambda 6087$ emission lines are detected. This implies the presence of intense X-ray emission in Tol 1214–277. In particular, to produce the observed [Fe VII] emission line fluxes and assuming that the X-ray sources are located in the compact region, the X-ray luminosity of the brightest H II region in Tol 1214–277 should be as high as $10^{39} - 10^{40}$ erg s $^{-1}$.

4. We find four emission-line galaxies in the field of Tol 1214–277, and four emission-line galaxies in the field of Tol 65. Seven of these galaxies are background star-forming galaxies with redshifts in the range 0.1 – 0.7. One emission-line galaxy in the field of Tol 1214–277 has the same redshift as the BCD and is likely a companion galaxy at a projected distance of ~ 14.5 kpc.

Acknowledgements. Y.I.I. acknowledges the Göttingen Academy of Sciences for a Gauss professorship. He and N.G.G. have been supported by DFG grant 436 UKR 17/22/03, by Swiss SCOPE 7UKPJ62178 grant and by grant No. 02.07/00132 of the Ukrainian fund for fundamental investigations. They are grateful for the hospitality of the Göttingen Observatory. P.P. and K.J.F. acknowledge support by the Volkswagen Foundation under grant No. I/72919. Y.I.I. and T.X.T. have been partially supported by NSF grant AST 02-05785. The research described in this publication was made possible in part by Award No. UP1-2551-KV-03 of the U.S. Civilian Research & Development Foundation for the Independent States of the Former Soviet Union (CRDF).

References

- Aller, L. H. 1984, *Physics of Thermal Gaseous Nebulae*, Dordrecht: Reidel
- Anders, E., & Grevesse, N. 1989, *Geochim.Cosmochim.Acta*, 53, 197
- Campbell, A., Terlevich, R., & Melnick, J. 1986, *MNRAS*, 223, 811

- Dopita, M. A., & Sutherland, R. S. 1996, *ApJS*, 102, 161
- Ferland, G. J. 1996, CLOUDY, Univ. of Kentucky, Dept. of Phys. and Astron. Internal Rep.
- Ferland, G. J., Korista, K. T., Verner, D. A., Ferguson, J. W., Kingdon, J. B., & Verner, E. M. 1998, *PASP*, 110, 761
- Fricke, K. J., Izotov, Y. I., Papaderos, P., Guseva, N. G., & Thuan, T. X. 2001, *AJ*, 121, 169
- Garnett, D. R. 1992, *AJ*, 103, 1330
- Guseva, N. G., Papaderos, P., Izotov, Y. I., Green, R. F., Fricke, K. J., Thuan, T. X., & Noeske, K. G. 2003, *A&A*, 407, 105
- Izotov, Y. I., & Thuan, T. X. 1998, *ApJ*, 500, 188
- Izotov, Y. I., & Thuan, T. X. 1999, *ApJ*, 511, 639
- Izotov, Y. I., & Thuan, T. X. 2004, *ApJ*, 602, 200
- Izotov, Y. I., Chaffee, F. H., & Green, R. F. 2001a, *ApJ*, 562, 727
- Izotov, Y. I., Chaffee, F. H., & Schaerer, D. 2001b, *A&A*, 378, L45
- Izotov, Y. I., Thuan, T. X., & Lipovetsky, V. A. 1994, *ApJ*, 435, 647
- Izotov, Y. I., Thuan, T. X., & Lipovetsky, V. A. 1997a, *ApJS*, 108, 1
- Izotov, Y. I., Lipovetsky, V. A., Chaffee, F. H., Foltz, C. B., Guseva, N. G., & Kniazev, A. Y. 1997b, *ApJ*, 476, 698
- Izotov, Y. I., Chaffee, F. H., Foltz, C. B., et al. 1999, *ApJ*, 527, 757
- Izotov, Y. I., Noeske, K. G., Guseva, N. G., Papaderos, P., Thuan, T. X., & Fricke, K. J. 2004, *A&A*, 415, L27
- Kurucz, R. L. 1979, *ApJS*, 40, 1
- Kunth, D., & Sargent, W. L. W. 1983, *ApJ*, 273, 81
- Lipovetsky, V. A., Chaffee, F. H., Izotov, Y. I., et al. 1999, *ApJ*, 519, 177
- Masegosa, J., Moles, M., & Campos-Aguilar, A. 1994, *ApJ*, 420, 576
- Meynet, G., & Maeder, A. 2002, *A&A*, 381, L25
- Noeske, K. G., Iglesias-Páramo, J., Vílchez, J. M., Papaderos, P., & Fricke, K. J. 2001, *A&A*, 371, 806
- Pagel, B. E. J., Simonson, E. A., Terlevich, R. J., & Edmunds, M. G. 1992, *MNRAS*, 255, 325
- Papaderos, P., Fricke, K. J., Thuan, T. X., Izotov, Y. I., & Nicklas, H. 1999, *A&A*, 352, L57
- Pustilnik, S. A., Brinks, E., Thuan, T. X., Lipovetsky, V. A., & Izotov, Y. I. 2001, *AJ*, 121, 1413
- Pustilnik, S. A., Lipovetsky, V. A., Izotov, Y. I., et al. 1997, *AstL*, 23, 308
- Pustilnik, S. A., Kniazev, A. Y., Pramskij, A. G., Ugryumov, A. V., & Masegosa, J. 2003, *A&A*, 409, 917
- Schaerer, D. 2002, *A&A*, 382, 28
- Schaerer, D. 2003, *A&A*, 397, 527
- Schaerer, D., & de Koter, A. 1997, *A&A*, 322, 598
- Smits, D. P. 1996, *MNRAS*, 278, 683
- Stasińska G. 1990, *A&AS*, 83, 501
- Thuan, T. X., & Izotov, Y. I. 1997, *ApJ*, 489, 623
- Thuan, T. X., Izotov, Y. I., & Lipovetsky, V. A. 1995, *ApJ*, 445, 108
- Thuan, T. X., Bauer, F. E., Papaderos, P., & Izotov, Y. I., 2004, *ApJ*, May 1
- Whitford, A.E. 1958, *AJ*, 63, 201